ROYAL SOCIETY
OF CHEMISTRY

PAPER

Check for updates

Enhanced stability of lead-free double perovskite Cs$_2$AgIn$_x$Bi$_{1-x}$Cl$_6$ crystals under a high humidity environment by surface capping treatment†

Jindou Shi, [iD] [a] Minqiang Wang,*[a] Chen Zhang,[a] Junnan Wang,[a] Yun Zhou,[a] Youlong Xu [iD] [a] and Nikolai V. Gaponenko[b]

Lead-free double perovskite (DP) crystals have received considerable attention for solving the toxicity and instability issues of traditional lead-based perovskites. However, recent studies have focused mainly on the improved optical performance of lead-free DP crystals, with less attention paid to their optical stability under high humidity environments. In this study, ligand-free lead-free DP Cs$_2$AgIn$_{0.93}$Bi$_{0.07}$Cl$_6$ nanocrystals (NCs) with excellent optical properties were prepared as research objects, and the larger surface area of the NCs caused them to be rapidly transformed into other phases after contact with water molecules, accompanied by a complete loss of optical properties, which significantly limited their application under high humidity environments. Therefore, surface capping treatment for Cs$_2$AgIn$_{0.93}$Bi$_{0.07}$Cl$_6$ NCs with an oleic acid (OA) ligand and polyvinylidene difluoride (PVDF) was proposed to achieve Cs$_2$AgIn$_{0.93}$Bi$_{0.07}$Cl$_6$ NCs-OA and Cs$_2$AgIn$_{0.93}$Bi$_{0.07}$Cl$_6$/PVDF composite films (CFs) with high water stability. In particular, the optically outstanding Cs$_2$AgIn$_{0.93}$Bi$_{0.07}$Cl$_6$/PVDF CFs exhibited stable fluorescence emission even after being stored in water solution for 10 days, and the assembled LED device operated well for a long time under 85% relative humidity (RH), which will bring a new dawn for the commercialization of next-generation lead-free DP optoelectronic devices.

Introduction

In recent years, lead halide perovskite nanocrystals (NCs) have been considered a star material in next generation optoelectronic devices due to their narrow bandwidth, high carrier mobility and coordinated emission, and have been widely applied in light emitting diodes (LEDs), photodetectors, solar cells, *etc.*[1–5] Unfortunately, the inherent toxicity of Pb^{2+} and instability under environmental conditions severely hinder its application in commercial fields, and therefore the replacement of Pb^{2+} with less toxic or non-toxic elements has become an effective solution that has received wide attention.[6–8] Commonly, divalent metal cations have been employed to isovalently replace Pb^{2+}, but they are highly susceptible to oxidation,[9,10] thus the synthesis of stable lead-free double perovskites (DPs) by heterovalent replacement with a combination of monovalent (B$^+$) and trivalent (B^{3+}) metal cations was considered promising.[11–13] However, in the existing reports of lead-free DP NCs, the researchers have been more concerned with the optimization of their optical properties,[14,15] rather than their optical stability in water medium, which will be detrimental to their application under some high humidity environments.

Recently, different lead-free DP materials have been obtained on the nanoscale using multiple synthetic routes.[16–19] Of these, the Cs$_2$AgBiX$_6$ (X = Cl, Br, I) DP material is valued for its high light absorption coefficient and improved photostability, and has been applied to alcohol-based photocatalytic systems and solar cells.[20–23] However, Cs$_2$AgBiX$_6$ exhibited weak PL emission, which was attributed to its indirect bandgap structure, severely limiting its application in lighting and display applications.[24–26] Fortunately, the photoluminescence (PL) properties of Cs$_2$AgBiX$_6$ have already been enhanced by strategies such as doping and alloying, allowing it to exhibit excellent fluorescence emission.[27–29] The co-doping of Yb^{3+} and Mn^{2+} in Cs$_2$AgBiX$_6$ (X = Cl, Br, I) was achieved by high temperature thermal injection, and double emission distribution at 680 nm and 1000 nm was observed in the optimized NCs.[30] Moreover, the band gap structure of Cs$_2$AgBiX$_6$ was induced to change from indirect to direct using an alloying strategy that utilized Ag$^+$ and Na$^+$ as B$^+$, thereby effectively boosting its photoluminescence

[a] *Electronic Materials Research Laboratory, Key Laboratory of the Ministry of Education International Center for Dielectric Research & Shannxi Engineering Research Center of Advanced Energy Materials and Devices, Xi'an Jiaotong University, 710049 Xi'an, China. E-mail: mqwang@xjtu.edu.cn*

[b] *Belarusian State University of Informatics and Radioelectronics, P. Browki 6, 220013 Minsk, Belarus*

† Electronic supplementary information (ESI) available. See DOI: https://doi.org/10.1039/d2tc05420e

4742 | *J. Mater. Chem. C*, 2023, **11**, 4742–4752

This journal is © The Royal Society of Chemistry 2023

quantum yields (PLQYs).[31] However, it has been reported that pure phase $Cs_2AgBiBr_6$ NCs can self-passivate to form BiOBr when immersed in water solution,[32] which will transform the crystal structure of $Cs_2AgBiBr_6$ NCs and consequently be devastating to the optical properties. Therefore, it is essential to investigate the optical stability of optimized Cs_2AgBiX_6 in water solution for its further development in the commercial field.

In this work, ligand-free $Cs_2AgBiCl_6$ NCs were acquired using a simple solvent-resistant recrystallisation method, and a subsequent strategy of adjusting the initial Bi/In metal precursors was adopted to complete the transformation for the band gap structure of $Cs_2AgBiCl_6$ from indirect to direct, resulting in ligand-free $Cs_2AgIn_{0.93}Bi_{0.07}Cl_6$ NCs with PLQYs of up to 19.72%. After that, the stability of ligand-free $Cs_2AgIn_{0.93}Bi_{0.07}Cl_6$ NCs under a high humidity environment was studied, and the results showed that $Cs_2AgIn_{0.93}Bi_{0.07}Cl_6$ NCs, with a larger surface area, rapidly transformed into other phases when in contact with water molecules, accompanied by the complete loss of optical properties, which greatly affects its practical application. Therefore, the surface capping treatment of $Cs_2AgIn_{0.93}Bi_{0.07}Cl_6$ using the oleic acid (OA) ligand and polyvinylidene difluoride (PVDF) was proposed, resulting in the preparation of $Cs_2AgIn_{0.93}Bi_{0.07}Cl_6$ NCs-OA and $Cs_2AgIn_{0.93}Bi_{0.07}Cl_6$/PVDF composite films (CFs) with enhanced water stability, respectively. In particular, the performance of $Cs_2AgIn_{0.93}Bi_{0.07}Cl_6$/PVDF CFs was outstanding, it still possessed a stable PL even after storage in pure water for 10 days, and the assembled LED devices operate well under 85% relative humidity (RH), which will significantly facilitate the development of lead-free DP materials in the future commercial lighting field.

Results and discussion

The preparation of lead-free DP NCs with uncapped surfaces by the antisolvent recrystallization method has been widely applied.[33,34] In this report, ligand-free $Cs_2AgIn_xBi_{1-x}Cl_6$ NCs with different feeding ratios were achieved by adjusting the ratio of the initial Bi/In metal precursors, and the structure and microscopic morphology of $Cs_2AgIn_xBi_{1-x}Cl_6$ NCs with different In^{3+} contents were investigated using X-ray diffraction (XRD) and transmission electron microscopy equipped with energy-dispersive spectroscopy (TEM-EDS). In order to obtain the actual doping ratio of In^{3+}, the elements in $Cs_2AgIn_xBi_{1-x}Cl_6$ NCs were quantitatively analyzed by inductively coupled plasma emission spectrometry (ICP-OES), and the results showed that the doping ratio increased as the feed amount of $InCl_3$ improved (Table S1, ESI†). The XRD patterns of $Cs_2AgIn_xBi_{1-x}Cl_6$ NCs with different In^{3+} contents revealed that all samples were highly crystalized in the DP crystal structure and that their diffraction peaks were located between bulk $Cs_2AgInCl_6$ (ICSD: 257115) and bulk $Cs_2AgBiCl_6$ (ICSD: 291598), in which no secondary phases were observed (Fig. 1a). Further observation of the XRD magnification in the $32°–36°$ range (Fig. 1b) revealed that the XRD peaks were shifted towards higher 2θ angles as the In^{3+} content in the $Cs_2AgIn_xBi_{1-x}Cl_6$ NCs

increased, and this result was attributed to the lattice contraction caused by the substitution of Bi^{3+} (ionic radius of 117 pm) with smaller In^{3+} (94 pm). Moreover, TEM images (Fig. 1c–f) of $Cs_2AgIn_xBi_{1-x}Cl_6$ NCs with different In^{3+} contents ($x = 0\%$, 73%, 97%, 100%) observed that the ligand-free NCs prepared using the antisolvent recrystallization method exhibit irregular nano blocky morphology. The morphologies of $Cs_2AgIn_xBi_{1-x}Cl_6$ NCs at other Bi/In ratios also present irregular nano blocks (Fig. S1, ESI†), so that the doping of In ions does not cause changes in the crystal morphology. Of these, the high-resolution TEM (HRTEM) images (insets of Fig. 1c and f) of $Cs_2AgBiCl_6$ NCs and $Cs_2AgInCl_6$ NCs revealed lattice spacings of 0.21 and 0.20 nm, corresponding to their (422) and (511) crystal planes, respectively. Finally, all elements were detected in the results of the EDS spectrum analysis of $Cs_2AgIn_{0.97}Bi_{0.03}Cl_6$ NCs doped with 97% In^{3+} (Fig. 1g), and their elemental mapping images revealed a homogeneous distribution of the different elements (Fig. 1h), which again supported the formation of alloy NCs. The above characterization results confirmed that the In^{3+} doping in $Cs_2AgBiCl_6$ NCs can be successfully achieved by this simple antisolvent recrystallization fabrication method.

The optical properties of $Cs_2AgIn_xBi_{1-x}Cl_6$ NCs with different In^{3+} contents were deeply investigated, enabling their better application for optoelectronic applications in the future. The UV-Vis absorbance spectrum of pure phase $Cs_2AgBiCl_6$ NCs showed a strong excitonic absorption peak at 370 nm, which was attributed to the s → p transition of Bi^{3+} (Fig. 2a).[35] In addition, the long sub-bandgap absorption tail of $Cs_2AgBiCl_6$ NCs at 400–700 nm (Fig. 2a and Fig. S2, ESI†) mainly originated from trap-state related transition and indirect bandgap transition.[33,34] Unfortunately, the indirect band gap transition belongs to the inherent properties of the materials that cannot be eliminated (Fig. 2c), which directly resulted in the lower fluorescence intensity of $Cs_2AgBiCl_6$ NCs (Fig. 2b and Fig. S3, ESI†). These results suggested that the indirect band gap of $Cs_2AgBiCl_6$ NCs greatly limited its application in the field of optoelectronic devices.[36] Similarly, the absorbance spectrum of the pure phase $Cs_2AgInCl_6$ NCs does not show a significant absorption peak (Fig. S4a, ESI†) and it exhibits a weak optical absorption coefficient around the band gap, corresponding to a lower PLQY value (Fig. S3 and S4b, ESI†), and therefore $Cs_2AgInCl_6$ NCs were also not a suitable candidate for optoelectronic materials. Here, the optical properties of $Cs_2AgIn_xBi_{1-x}Cl_6$ NCs with different Bi/In mix ratios were focused on. The absorbance spectra of all $Cs_2AgIn_xBi_{1-x}Cl_6$ NCs (x from 8% to 97%) exhibit an excitonic absorption peak at 370 nm originating from Bi^{3+} (Fig. 2a), and the absorption tail was effectively suppressed as the In content increased (Fig. 2a and Fig. S2, ESI†). In particular, at 97% doping of the In content, the band edges of the absorption spectra became sharp, indicating that $Cs_2AgIn_{0.97}Bi_{0.03}Cl_6$ NCs showed a direct band gap nature (Fig. 2c). At the same time, a progressively enhanced orange PL emission peak was observed at 570 nm with increasing In content (Fig. 2b and d), which derived from the self-trapping exciton (STE) state PL emission. The improvement of the optical properties resulted from the change in bandgap structure of $Cs_2AgIn_xBi_{1-x}Cl_6$ NCs, which gradually
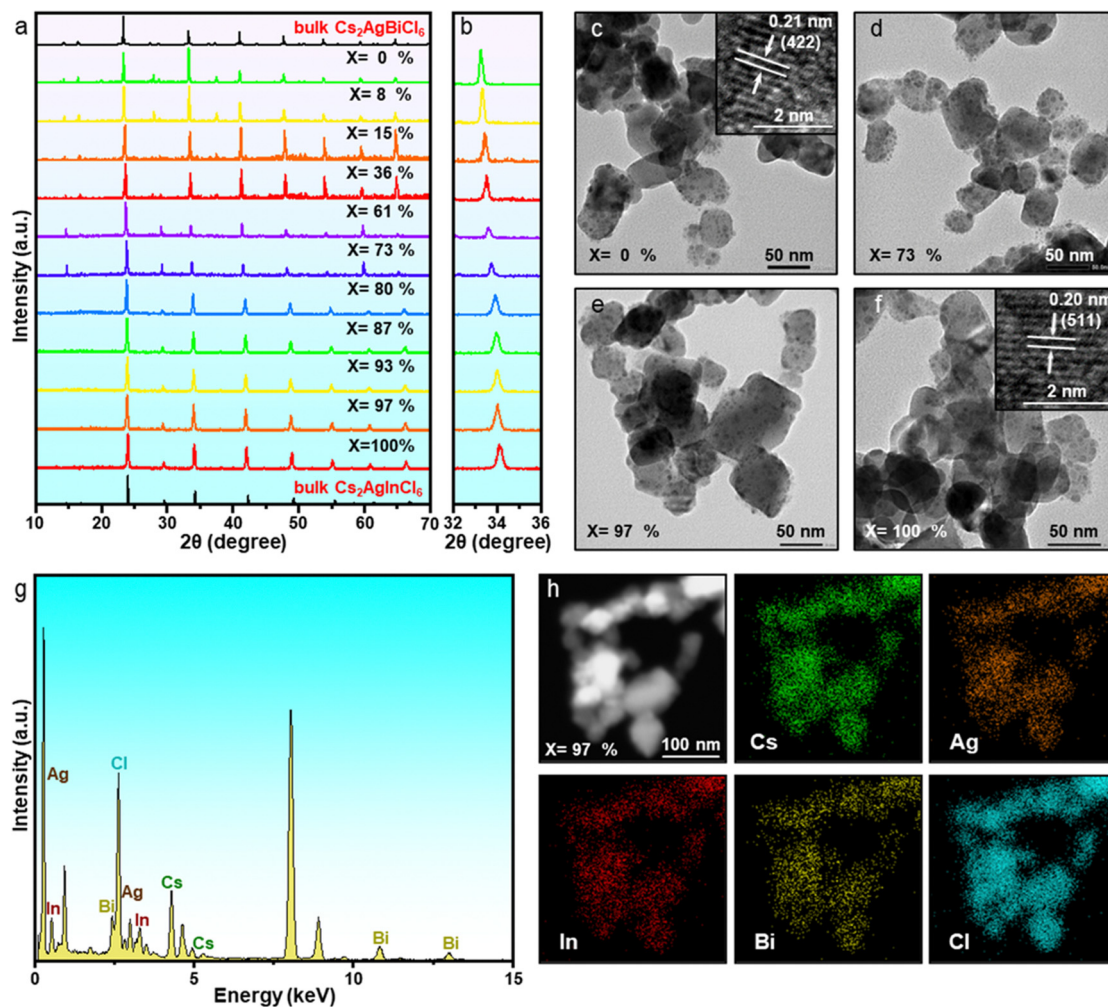
This journal is © The Royal Society of Chemistry 2023

J. Mater. Chem. C, 2023, **11**, 4742–4752 | **4743**

Fig. 1 (a) XRD patterns of $Cs_2AgIn_xBi_{1-x}Cl_6$ NCs with different In^{3+} contents (the bottom corresponds to a pure bulk $Cs_2AgInCl_6$ (ICSD: 257115) and the top to a pure bulk $Cs_2AgBiCl_6$ (ICSD: 291598). (b) Magnification of the XRD patterns in the $32°–36°$ range. TEM images of (c) $Cs_2AgBiCl_6$ NCs, (d) $Cs_2AgIn_{0.73}Bi_{0.27}Cl_6$ NCs, (e) $Cs_2AgIn_{0.97}Bi_{0.03}Cl_6$ NCs and (f) $Cs_2AgInCl_6$ NCs. (g) EDS spectrum and (h) elemental mapping of $Cs_2AgIn_{0.97}Bi_{0.03}Cl_6$ NCs. The insets in (c and f) display the corresponding HRTEM images.

transitioned from an indirect bandgap to a direct bandgap (Fig. 2c) with the continuous substitution of In^{3+}. Compared to indirect bandgap materials, the absorption and recombination processes in direct bandgap materials involve only photons and no phonon transfer (Fig. 2c),[37] thus achieving a PLQY of up to 19.72% for $Cs_2AgIn_{0.97}Bi_{0.03}Cl_6$ NCs (Fig. 2d and Fig. S3, ESI†). The lower PLQYs of NCs compared to those of some micron crystals (MCs) were due to the high crystallinity of the MCs,[38] but the large relative surface area of NCs provided more contact sites for subsequent studies of their optical stability under high humidity environments, making them more observable. In summary, ligand-free $Cs_2AgIn_{0.97}Bi_{0.03}Cl_6$ NCs ($Cs_2AgIn_{0.97}$-$Bi_{0.03}Cl_6$ NCs-free) with excellent optical properties were obtained by adjusting the initial mixing ratio of Bi/In metal precursors.

It is well known that the practical application of optoelectronic devices inevitably suffers from a high humidity environment,[39] and therefore further investigation about the stability of $Cs_2AgIn_{0.97}Bi_{0.03}Cl_6$ NCs-free in a water environment is more conducive to its commercialization. Here, the

$Cs_2AgIn_{0.97}Bi_{0.03}Cl_6$ NCs-free were transferred into a mixed solution of isopropanol and water (volume ratio of $8:2$) to simulate a high humidity environment, then the mixed solution under different reaction times was analyzed by XRD patterns, absorbance and PL spectra to investigate the change in water stability. The results indicated that $Cs_2AgIn_{0.97}Bi_{0.03}Cl_6$ NCs-free undisturbed by water molecules maintained its DP crystal structure (Fig. 3a), showing a strong exciton absorption peak at 370 nm (Fig. 3b) and emitting orange light of 570 nm under 365 nm UV light irradiation (Fig. 3c and d). Subsequently, the main crystal phase in the mixed solution changed rapidly with the addition of the water solution. The XRD pattern indicated that the characteristic diffraction peaks of $Cs_2AgIn_{0.97}Bi_{0.03}Cl_6$ NCs disappeared rapidly (1 min), which were replaced by many strong diffraction signals from AgCl and BiOCl, suggesting that the elements in $Cs_2AgIn_{0.97}Bi_{0.03}Cl_6$ NCs reacted with water molecules to transform into other phase substances (Fig. 3a). At the same time, the structural stability of $Cs_2AgBiCl_6$ NCs-free and $Cs_2AgInCl_6$ NCs-free was investigated
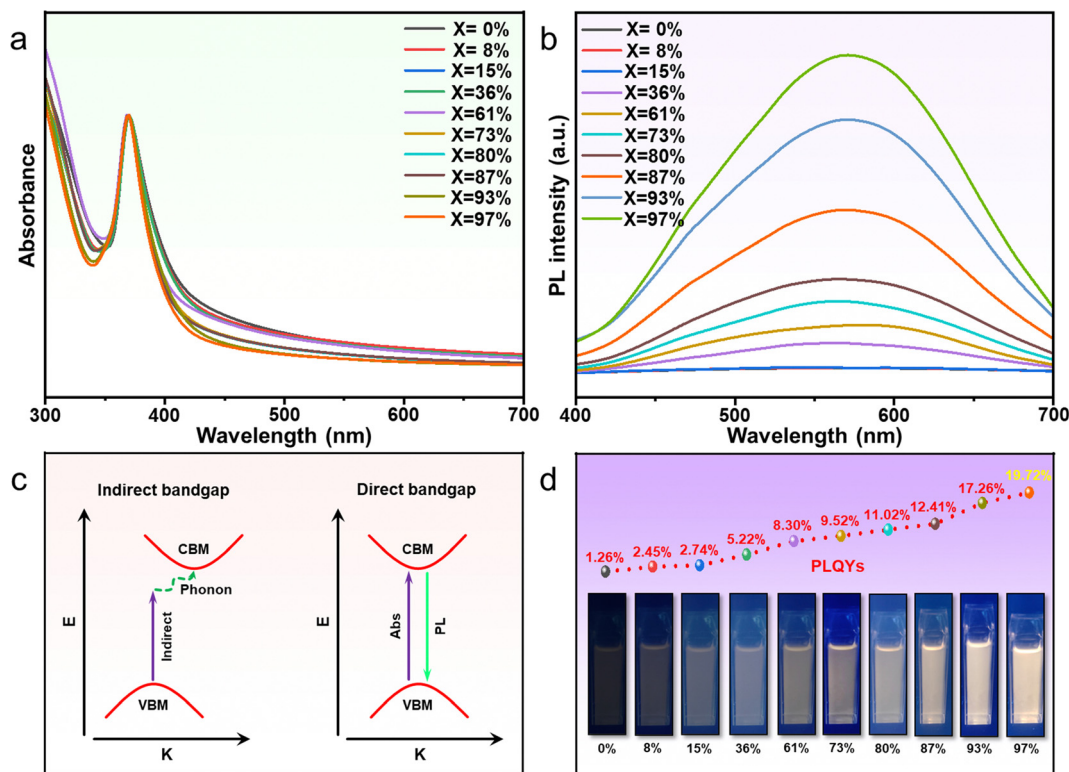
Fig. 2 (a) Absorbance and (b) PL spectra of $Cs_2AgIn_xBi_{1-x}Cl_6$ NCs as the In^{3+} content increased. (c) Schematic representation of the absorption and recombination processes between VBM and CBM for indirect bandgap (left) and direct bandgap (right) materials. (d) Photographs and PLQY values corresponding to $Cs_2AgIn_xBi_{1-x}Cl_6$ NCs with different In^{3+} content under a 365 nm UV light.

in the same mixed solution, respectively (Fig. S5, ESI†). After immersion in the mixed solution for 1 min, the XRD pattern showed that the diffraction peaks of BiOCl had completely occupied the positions of the pristine $Cs_2AgBiCl_6$, which was attributed to the element Bi in the $Cs_2AgBiCl_6$ NCs reacting with water molecules and transforming rapidly into the highly crystalline BiOCl (Fig. S5a, ESI†). A similar phenomenon has been reported in previous lead-free DP materials, where $Cs_2AgBiBr_6$ NCs fabricated by ligand-assisted recrystallisation were reacted with water molecules to transform into BiOBr.[32] After immersion of the ligand-free $Cs_2AgInCl_6$ NCs in the mixed solution for 1 min, the main crystal phase was rapidly transformed into AgCl (Fig. S5b, ESI†), by which time the $Cs_2AgInCl_6$ NCs had already decomposed, so that the presence of water molecules had a destructive effect on the structure of the $Cs_2AgIn_xBi_{1-x}Cl_6$ NCs-free. It can be concluded that $Cs_2AgIn_{0.97}Bi_{0.03}Cl_6$ NCs transformed into a mixed crystal phase of BiOCl and AgCl under high humidity, which resulted from the elemental Bi reacting with water molecules and the decomposition of the main crystal phase $Cs_2AgInCl_6$. Additionally, the optical properties of the $Cs_2AgIn_{0.97}Bi_{0.03}Cl_6$ NCs also suffered severe damage. With the addition of the water solution, the typical exciton absorption peak at 370 nm in the absorbance spectra of $Cs_2AgIn_{0.97}Bi_{0.03}Cl_6$ NCs disappeared (Fig. 3b), accompanied with the deterioration of the orange light emission intensity at 570 nm in their PL spectra (Fig. 3c), at which time the mixed solution exhibited no fluorescence under a

365 nm UV light (Fig. 3d). The elimination of the exciton absorption peak derived from the s → p transition in Bi^{3+} reconfirmed that the element Bi was consumed by the reaction with water, which destroyed the original band gap structure of $Cs_2AgIn_{0.97}Bi_{0.03}Cl_6$ NCs, leading directly to the deterioration of the optical properties. The above results indicated that the $Cs_2AgIn_{0.97}Bi_{0.03}Cl_6$ NCs-free readily react with water molecules to transform into BiOCl and AgCl with no optical properties, meaning that $Cs_2AgIn_{0.97}Bi_{0.03}Cl_6$ NCs-free would not be suitable for working in a high humidity environment, which severely limits its development in the field of optoelectronic devices. Therefore, solving the water stability problem of $Cs_2AgIn_{0.97}Bi_{0.03}Cl_6$ NCs-free will be an essential link to its subsequent exploitation.

To address the instability of $Cs_2AgIn_{0.97}Bi_{0.03}Cl_6$ NCs-free in a high humidity environment, a surface capping treatment with different materials was proposed, by referring to previous stability enhancement strategies of lead halide perovskites.[2,40] Based on the previously mentioned antisolvent recrystallization method, OA ligand capped $Cs_2AgIn_{0.97}Bi_{0.03}Cl_6$ NCs ($Cs_2AgIn_{0.97}Bi_{0.03}Cl_6$ NCs-OA) and $Cs_2AgIn_{0.97}Bi_{0.03}Cl_6$/PVDF composite films (CFs) were fabricated by employing oleic acid (OA) and polyvinylidene difluoride (PVDF) as surface capping materials, respectively (the detailed fabrication process can be found in the ESI†) (Fig. 4). As can be observed this treatment method was simple to operate, and suitable for large-scale production processes with great potential for application.
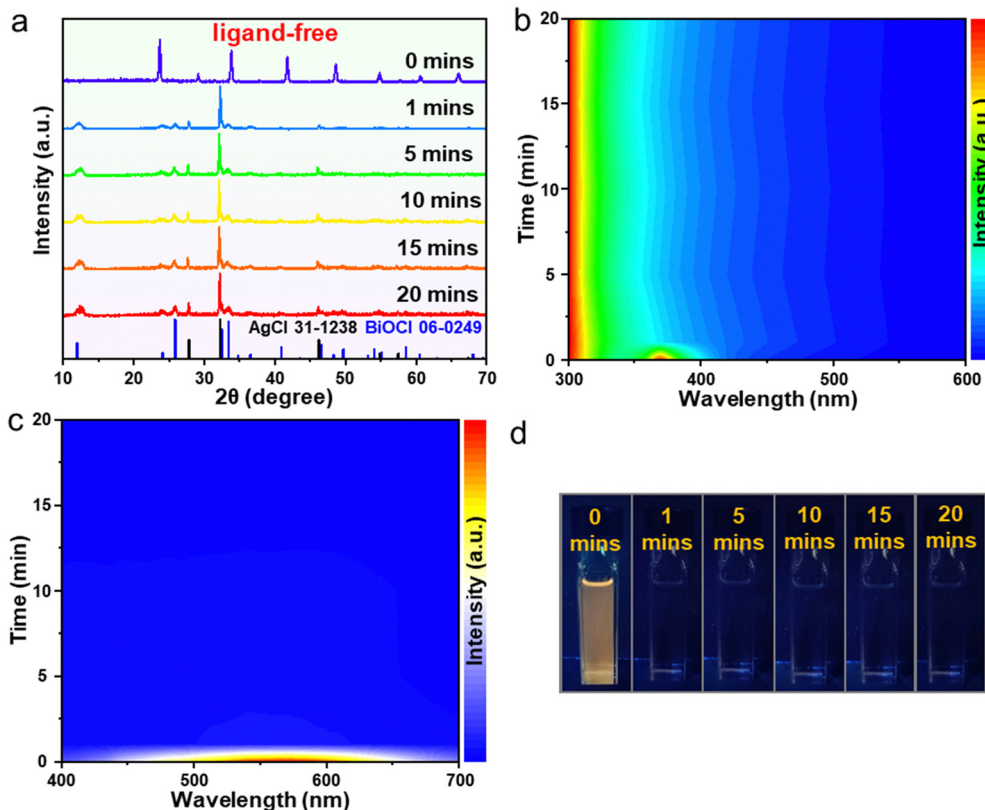
This journal is © The Royal Society of Chemistry 2023

J. Mater. Chem. C, 2023, **11**, 4742–4752 | **4745**

Fig. 3 (a) XRD patterns, (b) absorbance and (c) PL spectra of $Cs_2AgIn_{0.97}Bi_{0.03}Cl_6$ NCs-free at different times after water addition, and their photographs (d) under 365 nm UV light.

Further analysis was carried on the structure, morphology and optical properties of $Cs_2AgIn_{0.97}Bi_{0.03}Cl_6$ NCs-OA and $Cs_2AgIn_{0.97}Bi_{0.03}Cl_6$/PVDF CFs after the surface capping treatment. The XRD pattern of $Cs_2AgIn_{0.97}Bi_{0.03}Cl_6$ NCs-OA capped with the OA ligand showed no transformation in its crystalline phase and was consistent with $Cs_2AgIn_{0.97}Bi_{0.03}Cl_6$ NCs-free, both being highly crystalized in the DP crystal structure (Fig. 5a), indicating that the OA ligand was only adsorbed on the surface of $Cs_2AgIn_{0.97}Bi_{0.03}Cl_6$ NCs and did not cause a change in its structure. TEM image of $Cs_2AgIn_{0.97}Bi_{0.03}Cl_6$ NCs-OA exhibited the irregular nano blocky morphology of the NCs (Fig. 5b), which was highly concordant with the morphology of $Cs_2AgIn_{0.97}Bi_{0.03}Cl_6$ NCs-free in the previous section (Fig. 1e), reaffirming that the surface capping treatment of this OA ligand will not affect the synthesis of $Cs_2AgIn_{0.97}Bi_{0.03}Cl_6$ NCs. The HRTEM image (insets of Fig. 5b) reflected the corresponding lattice spacing of 0.23 nm for $Cs_2AgIn_{0.97}Bi_{0.03}Cl_6$ NCs-OA. Additionally, the EDS spectrum and elemental mapping images of $Cs_2AgIn_{0.97}Bi_{0.03}Cl_6$ NCs-OA revealed that all elements were being detected (Fig. S6, ESI†), which again supported the formation of alloy NCs. Similarly, all the diffraction signals of $Cs_2AgIn_{0.97}Bi_{0.03}Cl_6$ were clearly detected in the XRD pattern of $Cs_2AgIn_{0.97}Bi_{0.03}Cl_6$/PVDF CFs (Fig. 5a), indicating that highly crystalline $Cs_2AgIn_{0.97}Bi_{0.03}Cl_6$ crystals can be achieved using this synthetic route. Meanwhile, a broad diffraction peak located at 19° was found in the XRD pattern,

which is consistent with the diffraction peak position of the pure phase PVDF film acquired under the same preparation conditions (Fig. S7a, ESI†), indicating that this fabrication strategy can be used for the growth of $Cs_2AgIn_{0.97}Bi_{0.03}Cl_6$ crystals inside PVDF films. Of these, the XRD peaks of $Cs_2AgIn_{0.97}Bi_{0.03}Cl_6$ crystals were more intense, thus making the XRD peaks of PVDF appear weaker. Compared to the pure phase PVDF film (Fig. S7b, ESI†), the SEM image of $Cs_2AgIn_{0.97}Bi_{0.03}Cl_6$/PVDF CFs contained many additional small crystals with an average particle size of about 200 nm (Fig. 5c), which still showed an irregular shape (insets of Fig. 5c). Corresponding EDS analysis and elemental mapping have confirmed the irregular crystals belonging to $Cs_2AgIn_{0.97}Bi_{0.03}Cl_6$ crystals (Fig. S8, ESI†), with their relatively large particle size originating from annealing at high temperatures during the capping treatment. Finally, Fourier transform infrared (FTIR) spectroscopy was applied to analyze the different capping materials on the surface of the crystals (Fig. 5d). The absorption bands at 2925 and 2855 cm^{-1} of $Cs_2AgIn_{0.97}Bi_{0.03}Cl_6$ NCs-OA were attributed to the stretching vibration of $-CH_2-$, and the absorption bands at 1549 and 1454 cm^{-1} belong to the stretching vibration of COO (red line), which can confirm the presence of OA ligand on the $Cs_2AgIn_{0.97}Bi_{0.03}Cl_6$ NCs-OA surface.[41] The absorption band at 1402 cm^{-1} of $Cs_2AgIn_{0.97}Bi_{0.03}Cl_6$/PVDF CFs was derived from the stretching vibration of C–H, and the absorption bands at 1275 cm^{-1} and 1168 cm^{-1} corresponded to the

4746 | *J. Mater. Chem. C*, 2023, **11**, 4742–4752

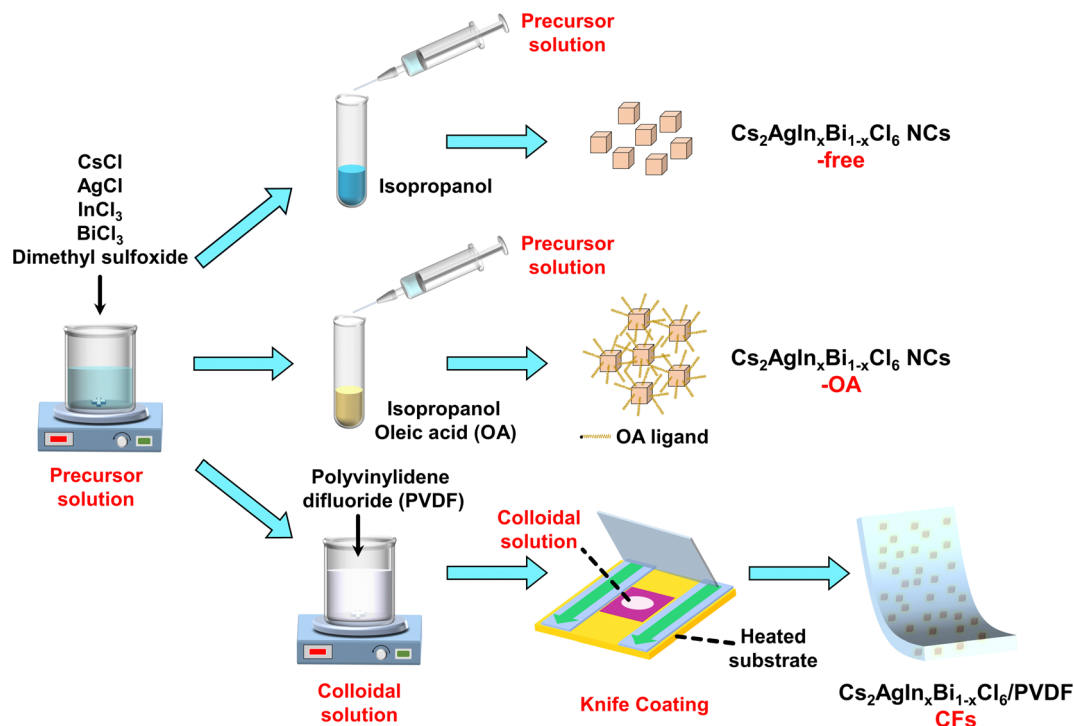This journal is © The Royal Society of Chemistry 2023

Fig. 4 Diagram of the surface capping treatment with different materials (ligand-free, OA ligand and PVDF).

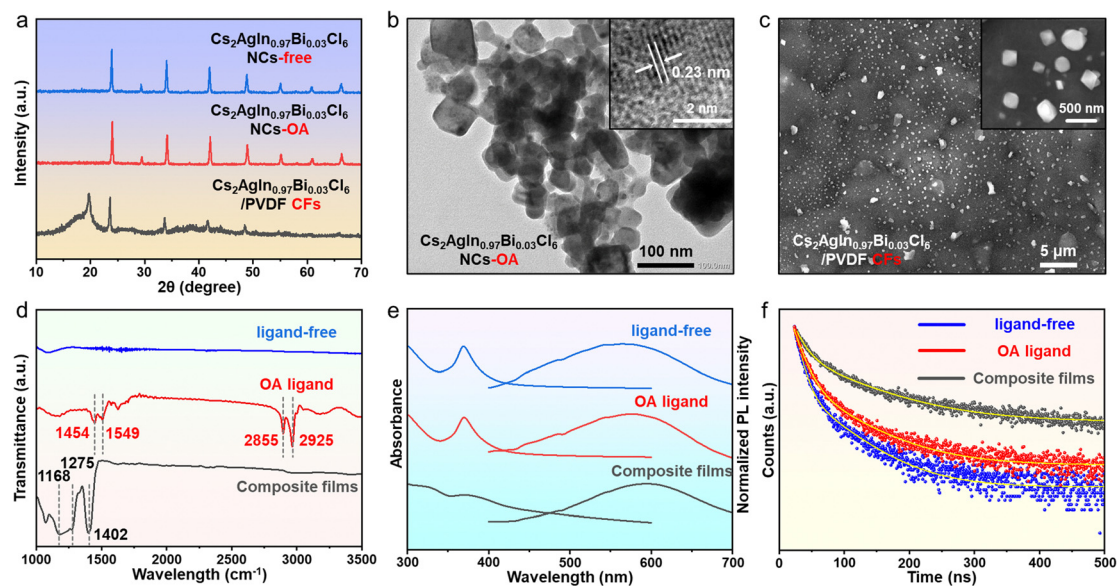**Fig. 5** (a) XRD patterns of three samples. (b) TEM image of $Cs_2AgIn_{0.97}Bi_{0.03}Cl_6$ NCs-OA. (c) SEM image of $Cs_2AgIn_{0.97}Bi_{0.03}Cl_6$/PVDF CFs. (d) FTIR, (e) absorbance, normalized PL and (f) time-resolved PL spectra of three samples. The inset in (b) displays the corresponding HRTEM image. The inset in (c) shows the corresponding locally enlarged SEM image.

stretching vibration of C–F (black line), which reflected the presence of PVDF on the $Cs_2AgIn_{0.97}Bi_{0.03}Cl_6$/PVDF CFs surface.[42] However, the characteristic bands of OA and PVDF were not detected in $Cs_2AgIn_{0.97}Bi_{0.03}Cl_6$ NCs-free (blue line), indicating the absence of protective layers on its surface. These characterization results confirm that high quality $Cs_2AgIn_{0.97}Bi_{0.03}Cl_6$ NCs-OA and $Cs_2AgIn_{0.97}Bi_{0.03}Cl_6$/PVDF

CFs were produced by surface capping for $Cs_2AgIn_{0.97}Bi_{0.03}Cl_6$ NCs with different materials (OA ligands and PVDF).

Subsequently, the changes in the optical properties of $Cs_2AgIn_{0.97}Bi_{0.03}Cl_6$ NCs-free, $Cs_2AgIn_{0.97}Bi_{0.03}Cl_6$ NCs-OA and $Cs_2AgIn_{0.97}Bi_{0.03}Cl_6$/PVDF CFs were compared. The absorption and PL spectra of $Cs_2AgIn_{0.97}Bi_{0.03}Cl_6$ NCs-OA are similar to those of $Cs_2AgIn_{0.97}Bi_{0.03}Cl_6$ NCs-free, benefiting from the fact

This journal is © The Royal Society of Chemistry 2023

J. Mater. Chem. C, 2023, **11**, 4742–4752 | **4747**

that the structure and morphology remain almost unchanged, and an intense exciton absorption peak can be clearly observed at 370 nm with the corresponding PL emission peak being also at 570 nm (Fig. 5e). On the other hand, the PVDF layer on the surface of $Cs_2AgIn_{0.97}Bi_{0.03}Cl_6$/PVDF CFs was too thick, resulting in the signal of its exciton absorption peak being partially masked, and a broad peak with weak intensity can be seen at 370 nm (Fig. 5e). The PL emission peak of $Cs_2AgIn_{0.97}Bi_{0.03}Cl_6$/PVDF CFs has been red-shifted to 593 nm, which can be attributed to the enlarged particle size, a similar phenomenon that has also been reported for lead halide perovskite materials (Fig. 5e).[43] In particular, the PLQYs of $Cs_2AgIn_{0.97}Bi_{0.03}Cl_6$ NCs-OA and $Cs_2AgIn_{0.97}Bi_{0.03}Cl_6$/PVDF CFs after surface capping were increased to 22.58% and 31.06%, respectively (Fig. S9, ESI†), which was explained by the fact that the surface defects of $Cs_2AgIn_{0.97}Bi_{0.03}Cl_6$ NCs can be effectively suppressed by the surface capping treatment.[33,34] Finally, to gain insight into the photophysics of the enhanced PLQY after surface capping treatment, the time-resolved PL decay behavior of the samples was recorded (Fig. 5f). The results revealed that the PL decay curves of all samples were well fitted by the bi-exponential decay function, where the fast decay was associated with trap-assisted recombination (τ_1), while the slow decay was associated with radiative recombination (τ_2).[44,45] From the data analysis it can be concluded that the surface capping treatment was able to change the ratio (A_1, A_2) of the two recombination types (Table S2, ESI†), resulting in an increase in the exciton

radiative recombination, which contributed to the improved PLQYs of $Cs_2AgIn_{0.97}Bi_{0.03}Cl_6$ NCs-OA and $Cs_2AgIn_{0.97}Bi_{0.03}Cl_6$/PVDF CFs. Combined with the above optical characteristic studies, the surface capping treatment can accomplish enhanced optical properties of $Cs_2AgIn_{0.97}Bi_{0.03}Cl_6$ NCs, which enable it to be more applicable to optoelectronic lighting systems.

The water stability of $Cs_2AgIn_{0.97}Bi_{0.03}Cl_6$ NCs after capping treatment with different materials was investigated, and changes in the structural and optical properties of $Cs_2AgIn_{0.97}Bi_{0.03}Cl_6$ NCs-OA were monitored in the same humidity environment (the volume ratio of isopropanol to water is 8 : 2), while $Cs_2AgIn_{0.97}Bi_{0.03}Cl_6$/PVDF CFs were placed in a harsher pure water environment (the volume ratio of isopropanol to water is 0 : 10) for observation. Benefiting from the protection of the surface OA ligand, so that $Cs_2AgIn_{0.97}Bi_{0.03}Cl_6$ NCs-OA did not exhibit loss of optical properties immediately after the water addition, the main crystal phase in the mixed solution remained as $Cs_2AgIn_{0.97}Bi_{0.03}Cl_6$ NCs (Fig. 6a). Unfortunately, the water solution gradually broke through the OA ligand on the surface of the $Cs_2AgIn_{0.97}Bi_{0.03}Cl_6$ NCs-OA as time progressed, which reacted with $Cs_2AgIn_{0.97}Bi_{0.03}Cl_6$ to produce other crystal phases. The XRD pattern displayed the diffraction peaks of BiOCl and AgCl when the mixed solution was stored for 5 min (Fig. 6a), but the diffraction intensity was lower at this time, indicating that only part of $Cs_2AgIn_{0.97}Bi_{0.03}Cl_6$ NCs-OA made contact with the water molecules. At the same time, the

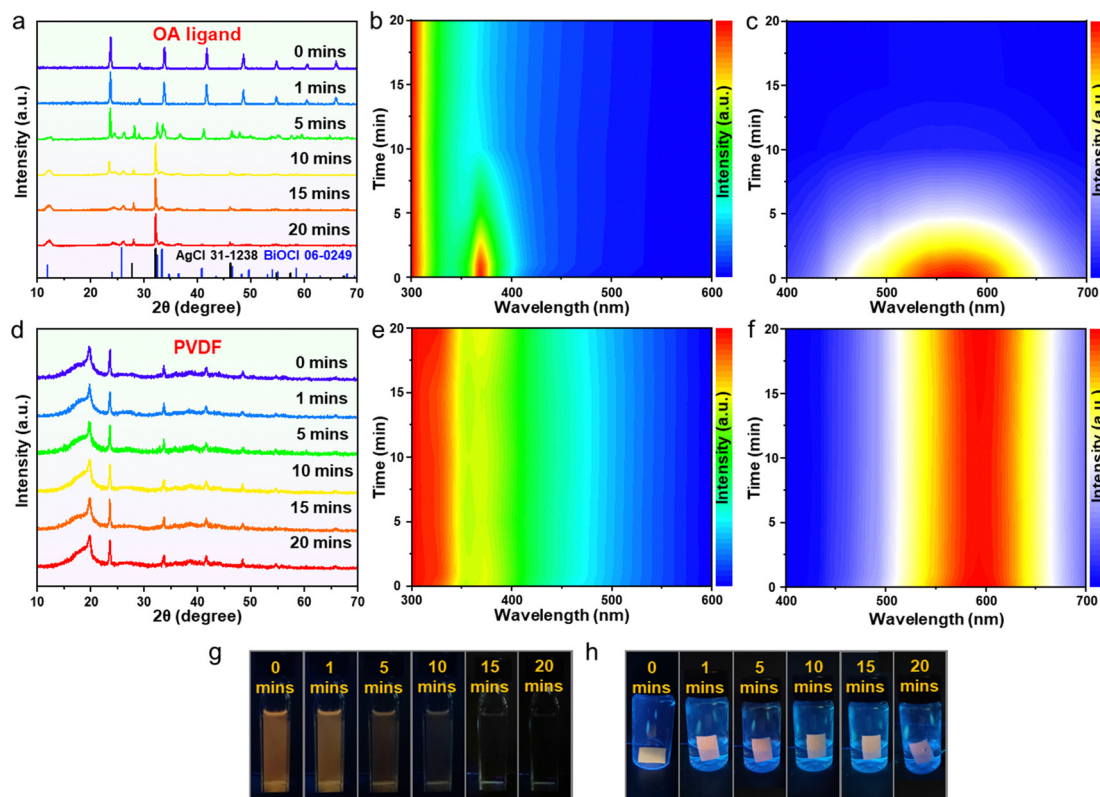**Fig. 6** (a and d) XRD patterns, (b and e) absorbance and (c and f) PL spectra of $Cs_2AgIn_{0.97}Bi_{0.03}Cl_6$ NCs-OA and $Cs_2AgIn_{0.97}Bi_{0.03}Cl_6$/PVDF CFs at different times after water addition, and their photographs (g and h) under 365 nm UV light.

4748 | *J. Mater. Chem. C*, 2023, **11**, 4742–4752

This journal is © The Royal Society of Chemistry 2023

exciton absorption peak intensity as well as the PL emission peak intensity of $Cs_2AgIn_{0.97}Bi_{0.03}Cl_6$ NCs-OA were weakened (Fig. 6b and c), and their corresponding fluorescence performance appeared to decline significantly (Fig. 6g). Especially, the XRD peaks of BiOCl and AgCl completely replaced the position of the pristine $Cs_2AgIn_{0.97}Bi_{0.03}Cl_6$ NCs-OA after the mixed solution was preserved for 15 min (Fig. 6a), and the exciton absorption peak of $Cs_2AgIn_{0.97}Bi_{0.03}Cl_6$ NCs-OA completely disappeared (Fig. 6b), corresponding to the fact that the PL emission signal was also not monitored (Fig. 6c), indicating that the water molecules had broken through the protective layer formed by the OA ligand on the surface of $Cs_2AgIn_{0.97}Bi_{0.03}Cl_6$ NCs. It can be concluded that surface capping of $Cs_2AgIn_{0.97}Bi_{0.03}Cl_6$ NCs with OA ligand does promote its water stability, but does not fundamentally solve the problem. The OA ligand on the surface of $Cs_2AgIn_{0.97}Bi_{0.03}Cl_6$ NCs-OA will fall off under prolonged storage, providing the opportunity for water molecules to make contact with $Cs_2AgIn_{0.97}Bi_{0.03}Cl_6$ NCs, thereby unable to guarantee the long-term fluorescence stability of $Cs_2AgIn_{0.97}Bi_{0.03}Cl_6$ NCs-OA in a high humidity environment (Fig. 6g), and a similar phenomenon has been reported previously for lead halide perovskite materials.[46] It is striking that the $Cs_2AgIn_{0.97}Bi_{0.03}Cl_6$/PVDF CFs with PVDF *in situ* capping treatment exhibited excellent stability after long-term storage in pure water solution. The water molecules can be effectively blocked from the surface of the CFs owing to the hydrophobicity of PVDF, inhibiting them from reacting with $Cs_2AgIn_{0.97}Bi_{0.03}Cl_6$, thereby significantly improving the structural and optical stability of $Cs_2AgIn_{0.97}Bi_{0.03}Cl_6$/PVDF CFs. The test results showed that the crystal phase of $Cs_2AgIn_{0.97}Bi_{0.03}Cl_6$/PVDF CFs did not change after storage in pure water for 20 min, which was attributed to the water molecules being unable to break through the PVDF film (Fig. 6d). The structural stability of $Cs_2AgIn_{0.97}Bi_{0.03}Cl_6$/PVDF CFs ensured that its optical properties were not affected (Fig. 6e and f), and it continued to exhibit orange fluorescence emission in water solution (Fig. 6h). Additionally, the ultra-long term water stability test was carried on $Cs_2AgIn_{0.97}Bi_{0.03}Cl_6$/PVDF CFs, and its structural and optical properties did not deteriorate after storage in water solution for ten days (Fig. S10, ESI†), which again established the development potential of $Cs_2AgIn_{0.97}Bi_{0.03}Cl_6$/PVDF CFs in the optoelectronic field. Combined with the above results, the surface capping treatment for $Cs_2AgIn_{0.97}Bi_{0.03}Cl_6$ NCs with different materials can indeed effectively improve its water stability, especially $Cs_2AgIn_{0.97}Bi_{0.03}Cl_6$/PVDF CFs capped with PVDF without any optical loss during long-term storage in water solution, which will lay the foundation for the subsequent development of lead-free DP optoelectronic devices under a high humidity environment.

In order to evaluate the working stability of lead-free DP materials with surface capping treatment in practical optoelectronic application, LED devices based on $Cs_2AgIn_{0.97}Bi_{0.03}Cl_6$ NCs-free, $Cs_2AgIn_{0.97}Bi_{0.03}Cl_6$ NCs-OA and $Cs_2AgIn_{0.97}Bi_{0.03}Cl_6$/PVDF CFs were assembled through directly coating the materials on the surface of a 365 nm UV chip (Fig. 7a). Saturation of the electroluminescence (EL) intensity was not observed in the three devices when the drive current was enhanced from 5 mA to 100 mA (Fig. S11a–c, ESI†), indicating that the LEDs assembled with lead-free DP materials were suitable for high power lighting systems. Moreover, the color rendering index (CRI) of the three LEDs remained essentially at a high value of 85, benefiting from the strong emission of the UV chip, and their correlated color temperature (CCT) also maintained a constant value (3400 K, 3400 K, 3600 K), which reflected that $Cs_2AgIn_{0.97}Bi_{0.03}Cl_6$ NCs-free, $Cs_2AgIn_{0.97}Bi_{0.03}Cl_6$ NCs-OA and $Cs_2AgIn_{0.97}Bi_{0.03}Cl_6$/PVDF CFs showed high emission purity at different drive currents (Fig. S11d–f, ESI†). By comparing the performance of LED devices based on other lead-free DP materials (Table S3, ESI†), it can be seen that our assembled LED devices also have excellent optoelectronic performances, making them strongly competitive for future commercial applications of lead-free DP materials. Subsequently, the working stability of the optoelectronic devices under a high humidity environment were investigated by placing LEDs assembled from different samples into a constant humidity test chamber. The relative humidity (RH) inside the test chamber was maintained at 85% to simulate the high humidity working environment of the devices, and the changes in their spectra and related optoelectronic parameters at different storage times were recorded (Fig. 7a). Undoubtedly, the optoelectronic properties of the LEDs assembled with $Cs_2AgIn_{0.97}Bi_{0.03}Cl_6$ NCs-free were most affected by the high humidity environment. Originating from the high content of water molecules in the environment, the drop tendency in the EL intensity of the device was most noticeable as the preservation time extended (Fig. 7b). The color coordinates in the international commission on illumination (CIE) diagram also shifted from the initial (0.39, 0.40) to (0.46, 0.41) after the LEDs had been stored under a high humidity environment for 24 h (Fig. S12a, ESI†), which was seriously inconsistent with the requirements of commercial lighting systems. At the same time, the CCT values varied between 3400 K and 3800 K of the device (Fig. 7e), which again suggested that the LEDs assembled with $Cs_2AgIn_{0.97}Bi_{0.03}Cl_6$ NCs-free were not suitable for stable optoelectronic devices with their emission light purity changing with operating time under a high humidity environment. On the other hand, the CRI values of the device stayed almost constant (Fig. 7e), which indicated that the bottom UV chip was not disturbed by humidity, thus excluding the influence of the excitation source on the optoelectronic properties of the lead-free DP materials. In comparison, the LEDs assembled with $Cs_2AgIn_{0.97}Bi_{0.03}Cl_6$ NCs-OA achieved a partial enhancement of long-term working stability under the same humidity environment. The results showed that the EL intensity loss began to be observed after storage for 8 h (Fig. 7c), and the corresponding color coordinates also exhibited a slightly fluctuating range (Fig. S12b, ESI†), which resulted from the fact that some OA ligands were broken through by water molecules as the time prolonged, thereby causing the emission of the device to be affected. Moreover, the CCT values of the LEDs also changed (from 3400 K to 3600 K), and their variation range has been controlled
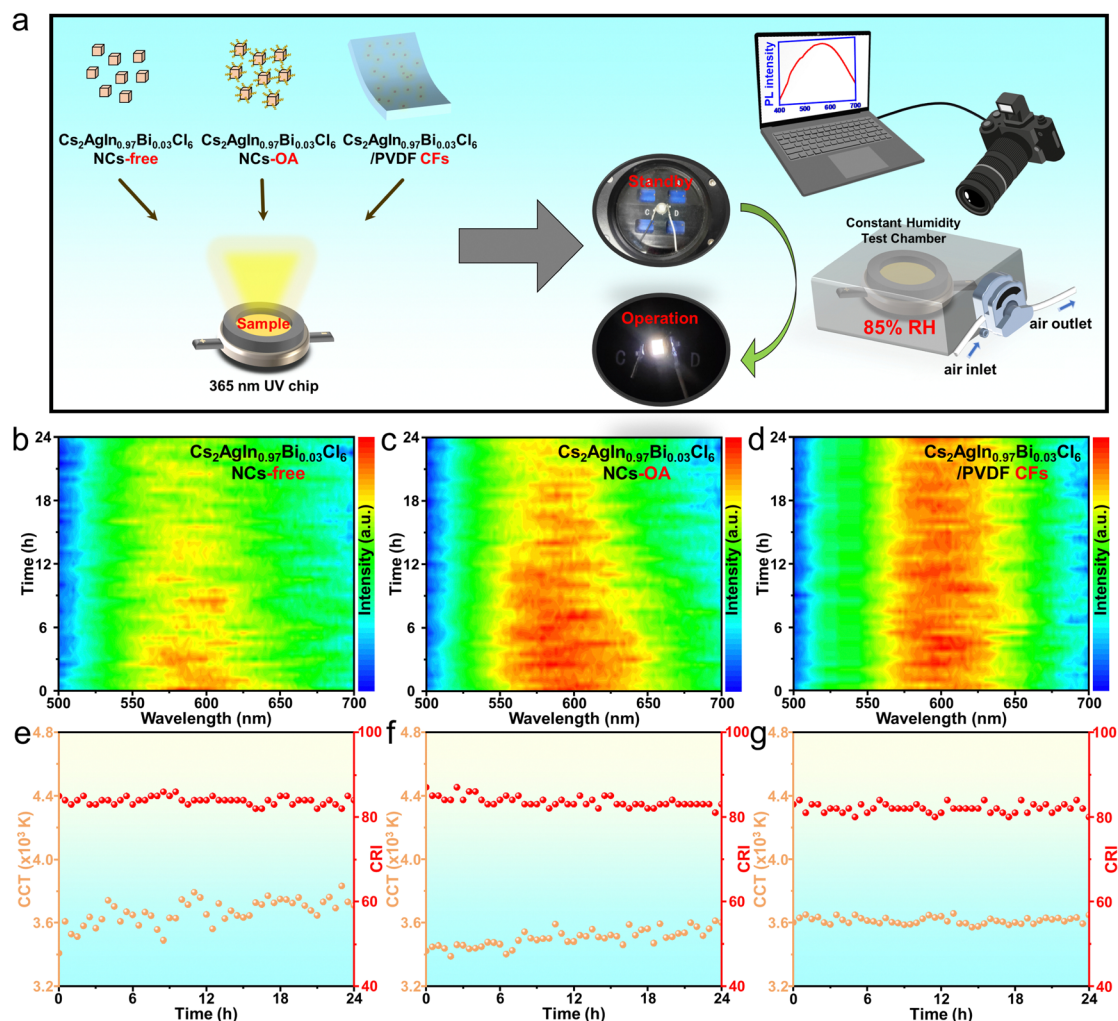
This journal is © The Royal Society of Chemistry 2023

J. Mater. Chem. C, 2023, **11**, 4742–4752 | **4749**

Fig. 7 (a) Diagram of the assembled LED devices using samples with different surface capping treatments and their operational stability tested under high humidity (85% RH) conditions. Changes in the (b–d) EL spectra, (e–g) CRI (red dot) and CCT (yellow dot) of the LEDs at different storage times.

compared to $Cs_2AgIn_{0.97}Bi_{0.03}Cl_6$ NCs-free (Fig. 7f), which demonstrated again the successful treatment of the OA ligand capping, resulting in an improved optical stability of the device under a high humidity environment. It was pleasantly surprising that the orange emitting LED assembled with $Cs_2AgIn_{0.97}Bi_{0.03}Cl_6$/PVDF CFs exhibited the most outstanding optoelectronic stability, which was stored in the constant humidity test chamber for 24 h without any loss of EL intensity (Fig. 7d), and the corresponding color coordinates remained at (0.41, 0.40), and no variation was observed over time (Fig. S12c, ESI†). Additionally, the CCT values of the device also remained essentially constant (3600 K) over a 24 h period (Fig. 7g), with the results showing a much smaller range of variation than the other two LEDs. From the practical optoelectronic applications of the above samples under high humidity, the $Cs_2AgIn_{0.97}$-$Bi_{0.03}Cl_6$/PVDF CFs after PVDF surface capping have a high working stability and can be better adapted to lighting systems under extreme environments, which will provide a new path to achieve efficient and stable lead-free DP devices.

Conclusions

In summary, we have acquired lead-free DP $Cs_2AgIn_{0.97}Bi_{0.03}Cl_6$ NCs-free with PLQYs of up to 19.72% by adjusting the ratio of Bi/In metal precursors, and investigated their optical stability under high humidity environments. Unfortunately, the $Cs_2AgIn_{0.97}Bi_{0.03}Cl_6$ NCs-free was rapidly transformed into AgCl and BiOCl with no fluorescent properties after being in contact with water molecules, accompanied by the quenching of the orange light emission. Therefore, we have proposed a surface capping treatment for $Cs_2AgIn_{0.97}Bi_{0.03}Cl_6$ NCs-free using the OA ligand and PVDF, which yielded $Cs_2AgIn_{0.97}Bi_{0.03}Cl_6$ NCs-OA and $Cs_2AgIn_{0.97}Bi_{0.03}Cl_6$/PVDF CFs with enhanced optical properties, corresponding to a PLQY of 22.58% and 31.06%, respectively. On this basis, the optical stability of $Cs_2AgIn_{0.97}$-$Bi_{0.03}Cl_6$ NCs-OA and $Cs_2AgIn_{0.97}Bi_{0.03}Cl_6$/PVDF CFs was compared under high humidity, benefiting from the surface capping material effectively preventing direct contact between $Cs_2AgIn_{0.97}Bi_{0.03}Cl_6$ NCs and water molecules, so that their stability was improved. In particular, the optical properties of

4750 | *J. Mater. Chem. C*, 2023, **11**, 4742–4752

This journal is © The Royal Society of Chemistry 2023

$Cs_2AgIn_{0.97}Bi_{0.03}Cl_6$/PVDF CFs were unaffected after storage in pure water solution for 10 days, and the fluorescence emission of the assembled LED device remained at the initial intensity after storage for 24 h at 85% RH. We believe that this strategy of surface capping with different materials will greatly facilitate the suitability of lead-free DP materials for various extreme environments, further broadening their application in future commercial lighting fields.

Author contributions

Jindou Shi: conceptualization (lead), investigation (lead), methodology (lead), and writing – original draft preparation (lead); Minqiang Wang: conceptualization (equal), funding acquisition (lead), and writing – review & editing (lead); Chen Zhang: investigation (equal); Junnan Wang: conceptualization (equal); Yun Zhou: investigation (equal); Youlong Xu: investigation (equal); Nikolai V. Gaponenko: investigation (equal).

Conflicts of interest

There are no conflicts to declare.

Acknowledgements

Notes and references

1 J. Z. Ye, M. M. Byranvand, C. O. Martnez, R. L. Z. Hoye, M. Saliba and L. Polavarapu, *Angew. Chem., Int. Ed.*, 2021, **60**, 21636–21660.

2 J. D. Shi, W. Y. Ge, Y. Tian, M. M. Xu, W. X. Gao and Y. T. Wu, *Small*, 2021, **17**, 2006568.

3 J. J. Yoo, G. Seo, M. R. Chua, T. G. Park, Y. L. Lu, F. Rotermund, Y. K. Kim, C. S. Moon, N. J. Jeon, J. P. Correa-Baena, V. Bulovic, S. S. Shin, M. G. Bawendi and J. Seo, *Nature*, 2021, **590**, 587–593.

4 Y. Z. Jiang, C. C. Qin, M. H. Cui, T. W. He, K. K. Liu, Y. M. Huang, M. H. Luo, L. Zhang, H. Y. Xu, S. S. Li, J. L. Wei, Z. Y. Liu, H. H. Wang, W. Kim, M. J. Yuan and J. Chen, *Nat. Commun.*, 2019, **10**, 1868.

5 M. G. Gong, R. Sakidja, R. Goul, D. Ewing, M. Casper, A. Stramel, A. Elliot and J. Z. Wu, *ACS Nano*, 2019, **13**, 1772–1783.

6 M. Ren, X. F. Qian, Y. T. Chen, T. F. Wang and Y. X. Zhao, *J. Hazard. Mater.*, 2022, **426**, 127848.

7 M. H. Wang, W. Wang, B. Ma, W. Shen, L. H. Liu, K. Cao, S. F. Chen and W. Huang, *Nano-Micro Lett.*, 2021, **13**, 62.

8 Z. X. Li, P. Wang, C. Ma, F. Igbari, Y. K. Kang, K. L. Wang, W. Y. Song, C. Dong, Y. J. Li, J. S. Yao, D. Meng, Z. K. Wang and Y. Yang, *J. Am. Chem. Soc.*, 2021, **143**, 2593–2600.

9 T. C. Jellicoe, J. M. Richter, H. F. Glass, M. Tabachnyk, R. Brady, S. N. E. Dutton, A. Rao, R. H. Friend, D. Credgington and N. C. Greenham, *J. Am. Chem. Soc.*, 2016, **138**, 2941–2944.

10 T. Krishnamoorthy, H. Ding, C. Yan, W. L. Leong, T. Baikie, Z. Y. Zhang, M. Sherburne, S. Li, M. Asta, N. Mathews and S. G. Mhaisalkar, *J. Mater. Chem. A*, 2015, **3**, 23829–23832.

11 F. Igbari, Z. K. Wang and L. S. Liao, *Adv. Energy Mater.*, 2019, **9**, 1803150.

12 Y. Liu, A. Nag, L. Manna and Z. G. Xia, *Angew. Chem., Int. Ed.*, 2021, **60**, 11592–11603.

13 J. C. Dahl, W. T. Osowiecki, Y. Cai, J. K. Swabeck, Y. Bekenstein, M. Asta, E. M. Chan and A. P. Alivisatos, *Chem. Mater.*, 2019, **31**, 3134–3143.

14 P. Han, X. Mao, S. Yang, F. Zhang, B. Yang, D. Wei, W. Deng and K. Han, *Angew. Chem., Int. Ed.*, 2019, **58**, 17231–17235.

15 Y. Liu, X. M. Rong, M. Z. Li, M. S. Molokeev, J. Zhao and Z. G. Xia, *Angew. Chem., Int. Ed.*, 2020, **59**, 11634–11640.

16 M. Wang, P. Zeng, Z. H. Wang and M. Z. Liu, *Adv. Sci.*, 2020, **7**, 1903662.

17 B. Zhou, Z. X. Liu, S. F. Fang, H. Z. Zhong, B. B. Tian, Y. Wang, H. N. Li, H. L. Hu and Y. M. Shi, *ACS Energy Lett.*, 2021, **6**, 3343–3351.

18 J. H. Nie, H. A. Li, S. F. Fang, B. Zhou, Z. X. Liu, F. M. Chen, Y. Wang and Y. M. Shi, *Cell Rep. Phys. Sci.*, 2022, **3**, 100820.

19 M. M. Yao, L. Wang, J. S. Yao, K. H. Wang, C. Chen, B. S. Zhu, J. N. Yang, J. J. Wang, W. P. Xu, Q. Zhang and H. B. Yao, *Adv. Opt. Mater.*, 2020, **8**, 1901919.

20 Z. Z. Zhang, Y. Q. Liang, H. L. Huang, X. Y. Liu, Q. Li, L. X. Chen and D. S. Xu, *Angew. Chem., Int. Ed.*, 2019, **58**, 7263–7267.

21 F. Igbari, R. Wang, Z. K. Wang, X. J. Ma, Q. Wang, K. L. Wang, Y. Zhang, L. S. Liao and Y. Yang, *Nano Lett.*, 2019, **19**, 2066–2073.

22 B. N. Wang, N. Li, L. Yang, C. Dall'Agnese, A. K. Jena, S. Sasaki, T. Miyasaka, H. Tamiaki and X. F. Wang, *J. Am. Chem. Soc.*, 2021, **143**, 2207–2211.

23 H. L. Wu, X. B. Li, C. H. Tung and L. Z. Wu, *Adv. Mater.*, 2019, **31**, 1900709.

24 S. Ghosh and B. Pradhan, *ChemNanoMat*, 2019, **5**, 300–312.

25 E. T. McClure, M. R. Ball, W. Windl and P. M. Woodward, *Chem. Mater.*, 2016, **28**, 1348–1354.

26 B. Yang, X. Mao, F. Hong, W. W. Meng, Y. X. Tang, X. S. Xia, S. Q. Yang, W. Q. Deng and K. L. Han, *J. Am. Chem. Soc.*, 2018, **140**, 17001–17006.

27 Y. F. Pei, D. T. Tu, C. L. Li, S. Y. Han, Z. Xie, F. Wen, L. P. Wang and X. Y. Chen, *Angew. Chem., Int. Ed.*, 2022, **61**, e202205276.

28 Z. C. Zeng, B. L. Huang, X. Wang, L. Lu, Q. Y. Lu, M. Z. Sun, T. Wu, T. F. Ma, J. Xu, Y. S. Xu, S. Wang, Y. P. Du and C. H. Yan, *Adv. Mater.*, 2020, **32**, 2004506.

29 D. X. Zhu, J. Zito, V. Pinchetti, Z. Y. Dang, A. Olivati, L. Pasquale, A. W. Tang, M. L. Zaffalon, F. Meinardi, I. Infante, L. De Trizio, L. Manna and S. Brovelli, *ACS Energy Lett.*, 2020, **5**, 1840–1847.

30 N. Chen, T. Cai, W. H. Li, K. Hills-Kimball, H. J. Yang, M. D. Que, Y. Nagaoka, Z. Y. Liu, D. Yang, A. G. Dong, C. Y. Xu, R. Zia and O. Chen, *ACS Appl. Mater. Interfaces*, 2019, **11**, 16855–16863.

31 F. Locardi, E. Sartori, J. Buha, J. Zito, M. Prato, V. Pinchetti, M. L. Zaffalon, M. Ferretti, S. Brovelli, I. Infante, L. De Trizio and L. Manna, *ACS Energy Lett.*, 2019, **4**, 1976–1982.

32 Q. Q. Fan, S. Y. Wei, J. Z. Ma, W. B. Zhang and L. Wen, *J. Mater. Chem. A*, 2022, **10**, 14923–14932.

33 B. Yang, J. S. Chen, F. Hong, X. Mao, K. B. Zheng, S. Q. Yang, Y. J. Li, T. Pullerits, W. Q. Deng and K. L. Han, *Angew. Chem., Int. Ed.*, 2017, **56**, 12471–12475.

34 B. Yang, J. S. Chen, S. Q. Yang, F. Hong, L. Sun, P. G. Han, T. Pullerits, W. Q. Deng and K. L. Han, *Angew. Chem., Int. Ed.*, 2018, **57**, 5359–5363.

35 Y. Bekenstein, J. C. Dahl, J. M. Huang, W. T. Osowiecki, J. K. Swabeck, E. M. Chan, P. D. Yang and A. P. Alivisatos, *Nano Lett.*, 2018, **18**, 3502–3508.

36 G. Volonakis, M. R. Filip, A. A. Haghighirad, N. Sakai, B. Wenger, H. J. Snaith and F. Giustino, *J. Phys. Chem. Lett.*, 2016, **7**, 1254–1259.

37 E. M. Hutter, M. C. Gelvez-Rueda, A. Osherov, V. Bulovic, F. C. Grozema, S. D. Stranks and T. J. Savenije, *Nat. Mater.*, 2017, **16**, 115–120.

38 O. Stroyuk, O. Raievska, A. Barabash, C. Kupfer, A. Osvet, V. Dzhagan, D. R. T. Zahn, J. Hauch and C. J. Brabec, *Mater. Adv.*, 2022, **3**, 7894–7903.

39 D. Di Girolamo, M. I. Dar, D. Dini, L. Gontrani, R. Caminiti, A. Mattoni, M. Graetzel and S. Meloni, *J. Mater. Chem. A*, 2019, **7**, 12292–12302.

40 J. D. Shi, W. Y. Ge, W. X. Gao, M. M. Xu, J. F. Zhu and Y. X. Li, *Adv. Opt. Mater.*, 2020, **8**, 1901516.

41 R. F. Li, X. D. Fang, J. L. Ren, B. J. Chen, X. Y. Yuan, X. C. Pan, P. Zhang, L. T. Zhang, D. T. Tu, Z. L. Fang, X. Y. Chen and Q. Ju, *Nanoscale*, 2021, **13**, 12494–12504.

42 Z. P. Zeng, D. S. Yu, Z. M. He, J. Liu, F. X. Xiao, Y. Zhang, R. Wang, D. Bhattacharyya and T. T. Y. Tan, *Sci. Rep.*, 2016, **6**, 20142.

43 J. D. Shi, Y. Tian, W. X. Gao, M. M. Xu, Y. T. Wu and W. Y. Ge, *ACS Appl. Electron. Mater.*, 2021, **3**, 1413–1421.

44 D. Shi, V. Adinolfi, R. Comin, M. J. Yuan, E. Alarousu, A. Buin, Y. Chen, S. Hoogland, A. Rothenberger, K. Katsiev, Y. Losovyj, X. Zhang, P. A. Dowben, O. F. Mohammed, E. H. Sargent and O. M. Bakr, *Science*, 2015, **347**, 519–522.

45 H. C. Cho, S. H. Jeong, M. H. Park, Y. H. Kim, C. Wolf, C. L. Lee, J. H. Heo, A. Sadhanala, N. Myoung, S. Yoo, S. H. Im, R. H. Friend and T. W. Lee, *Science*, 2015, **350**, 1222–1225.

46 J. D. Shi, W. Y. Ge, J. F. Zhu, M. Saruyama and T. Teranishi, *ACS Appl. Nano Mater.*, 2020, **3**, 7563–7571.

4752 | *J. Mater. Chem. C*, 2023, **11**, 4742–4752

This journal is © The Royal Society of Chemistry 2023